

# Implicit Two-Tower Policies

Yunfan Zhao \*  
Columbia University

Qingkai Pan \*  
Columbia University

Krzysztof Choromanski \*  
Google Brain & Columbia University

Deepali Jain  
Google Brain

Vikas Sindhwani  
Google Brain

## Abstract

We present a new class of structured reinforcement learning policy-architectures, *Implicit Two-Tower (ITT)* policies, where the actions are chosen based on the attention scores of their learnable latent representations with those of the input states. By explicitly disentangling action from state processing in the policy stack, we achieve two main goals: substantial computational gains and better performance. Our architectures are compatible with both discrete and continuous action spaces. By conducting tests on 15 environments from OpenAI Gym and DeepMind Control Suite, we show that ITT-architectures are particularly suited for black-box/evolutionary optimization and the corresponding policy training algorithms outperform their vanilla unstructured implicit counterparts as well as commonly used explicit policies. We complement our analysis by showing how techniques such as hashing and lazy tower updates, critically relying on the two-tower structure of ITTs, can be applied to obtain additional computational improvements.

## 1 Introduction & related work

We consider the problem of training a policy  $\pi_\theta : \mathcal{S} \rightarrow \mathcal{A}$ , parameterized by learnable  $\theta \in \mathbb{R}^D$  for a reinforcement learning (RL) agent ([29, 28, 1]). The policy is a potentially stochastic mapping from the state-space ( $\mathcal{S}$ ) to the action-space ( $\mathcal{A}$ ), either continuous or discrete. The objective is to maximize the expected total reward  $R$  defined as a possibly discounted sum of the partial rewards  $r_i(\mathbf{s}_i, \mathbf{a}_i, \mathbf{s}_{i+1})$  for the transition from  $\mathbf{s}_i \in \mathcal{S}$  to  $\mathbf{s}_{i+1} \in \mathcal{S}$  via  $\mathbf{a}_i \in \mathcal{A}$ . The transition function:  $T : \mathcal{S} \times \mathcal{A} \rightarrow \mathcal{S}$  as well as the partial reward function:  $r : \mathcal{S} \times \mathcal{A} \times \mathcal{S} \rightarrow \mathbb{R}$  (both potentially stochastic) are defined by the environment. Hence, expected total rewards are computed over random state transitions and action choices. We call the sequence  $(\mathbf{s}_0, \mathbf{a}_0, \mathbf{s}_1, \mathbf{a}_1, \dots, \mathbf{s}_T)$  of states visited by the agent intertwined with the actions proposed by  $\pi_\theta$ , the *rollout* of an agent.

The most common way of encoding policy mapping  $\pi_\theta$  is via a neural network taking states as inputs and explicitly outputting as the activations of the last layer proposed actions or the distributions over actions to sample from (for stochastic policies). We call such policies *explicit*. While explicit policies were successfully applied in several RL scenarios: learning directly from pixels, hierarchical learning, robot locomotion and more ([23, 22, 12, 6, 33, 14]), recent evidence shows that the expressiveness of the policy-architecture can be improved if the explicit model is substituted by an *implicit* one.

The implicit model ([13, 10, 9]) operates by learning a function  $E_\theta : \mathcal{S} \times \mathcal{A} \rightarrow \mathbb{R}$  taking as an input a state-action pair and outputting a scalar value that can be interpreted as an energy. The optimal action  $\mathbf{a}^*(\mathbf{s})$  for a given state  $\mathbf{s}$  is chosen as a solution to the following energy-minimization problem:

$$\mathbf{a}^*(\mathbf{s}) = \pi_\theta(\mathbf{s}) = \operatorname{argmin}_{\mathbf{a} \in \mathcal{A}} E_\theta(\mathbf{s}, \mathbf{a}). \quad (1)$$

---

\*Equal Contribution

Implicit models were recently demonstrated to provide strong performance in the behavioral cloning (BC) setting ([10]), outperforming their regular explicit counterparts (e.g. mean squared error and mixture density BC policies), also for high-dimensional action-spaces and image inputs. Interestingly, robots with deployed implicit policies were shown to learn sophisticated behaviours on various manipulation tasks requiring very high precision ([10]).

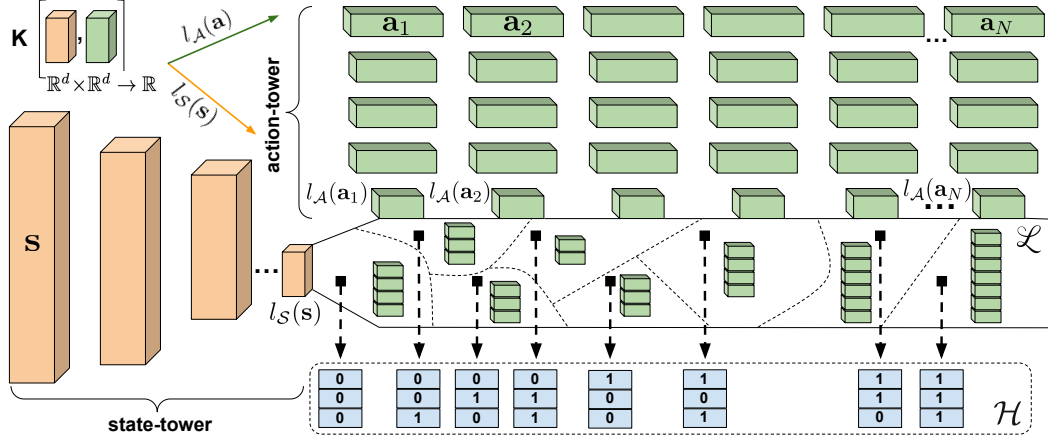


Figure 1: The conceptual description of the Implicit Two-Tower (ITT) stack. The (orange) state-tower and (green) action-tower map states  $s$  and actions  $a$  into their corresponding latent representations  $l_S(s), l_A(a) \in \mathbb{R}^d$ . The latent space  $\mathcal{L}$  can be itself partitioned into subregions, for instance via hashing mechanisms, for the sublinear approximate state-action match. This potential partitioning would need to be periodically updated in the training process, but in principle could be frozen in inference (if a fixed set of sampled actions is being applied). The energy-function is defined via a simple kernel  $K: \mathbb{R}^d \times \mathbb{R}^d \rightarrow \mathbb{R}$  acting on the latent representations.

New results, showing that the implicit mappings from states to actions given by Eq. 1 are capable of modeling multi-valued and even discontinuous functions with arbitrary precision (see: Theorem 1 and 2 in [10], and [3]) with continuous energy-functions  $E$  modeled by regular neural networks, shed light on that phenomenon. Thus adding the argmin-operator provides a gateway to extend universal approximation results of regular neural networks to larger classes of functions.

In the standard implementation of the implicit policies (see for instance: [10]), that we will refer to as the *implicit one-tower* (IOT) policies, the state and action feature vectors are concatenated and such an input is given to the energy-network. While seemingly natural, this approach has one crucial weakness - it is prohibitively expensive for large action-spaces. It requires solving nontrivial optimization argmin-problem at every state-to-state transition without opportunity to at least partially reuse computations conducted in the past. Indeed, even if the same actions are probed for different transitions (e.g. when the action-space has moderate cardinality or sampling heuristics are applied and the same sets of action samples are applied across different state-transitions) those actions are concatenated with different states leading to different inputs to the energy-function for different transitions. That is why in practice implicit policies apply sampling techniques with relatively few samples, affecting the quality of the approximation of the original optimization argmin-problem.

To address this key limitation, we introduce a new class of implicit policies architectures, called *implicit two-towers* (ITTs) (Fig. 1), where action processing is explicitly disentangled from state processing via the architectural design. The ITT-architecture consists of two towers mapping states and actions to the same  $d$ -dimensional latent space  $\mathcal{L}$ . The negated energy  $-E$  is then defined as a relatively simple kernel  $K: \mathbb{R}^d \times \mathbb{R}^d \rightarrow \mathbb{R}$  acting on the state/action latent representations (e.g. dot-product or softmax kernel). Such a representation has several computational advantages:

- it makes it possible to reuse computations conducted for a fixed set of actions (in the form of their latent representations) across different transitions within a rollout or even different rollouts; computational gains are present even if actions are sampled at every transition since in ITTs (as opposed to IOTs) action-processing is completely disentangled from the expensive state-transitions of the environment and thus latent representations of actions can be pre-computed before they are actually applied,
- it allows for action and state towers to be updated in different rates in training (e.g. less-frequent *lazy action-tower updates*) (see: Sec. 2.3),

- it is compatible with various approximate sublinear-time algorithms for solving the optimization argmin-problem in its new two-tower form (see: Sec 2.3.1).

ITTs can in particular apply a rich set of techniques for solving the maximum inner product (MIP) problem [18, 25, 24, 19], such as LSH-hashing, as well as algorithms conducting sub-linear softmax-sampling via linearization of the softmax kernel with random feature trees [4, 21]. Interestingly, they also produce policies obtaining larger rewards as compared to their IOT and explicit counterparts, as we demonstrate in Sec. 3 on 15 environments taken from OpenAI Gym and DeepMind Control Suite. ITTs can be applied for both: discrete and continuous action-spaces.

**ITTs with ES:** We decided to train parameters of our ITT-architectures with the class of Evolutionary Search (ES, Blackbox) methods ([22, 6, 17, 5]). Even though ITTs are agnostic to the particular training algorithm, ES-methods constituted a particularly attractive option. They enabled us to benchmark implicit policies in the on-policy setting, where to the best of our knowledge they were never tried before. Furthermore, as embarrassingly simple conceptually (yet very efficient at the same time), they let us focus on the architectural aspects rather than tedious hyperparameter-tuning. Finally, they work very well also with non-differentiable or even non-continuous objectives, fitting well the combinatorial-flavor of the energy optimization problem formulation in ITTs.

The implicit policies are intrinsically related to several classes of methods developed for machine learning (ML) and robotics. We review some of them below.

**Q-learning:**  $Q$ -learning methods ([11, 32, 30, 15]), that are prominent examples of the off-policy RL algorithms, can be thought of as instantiations of the implicit policies techniques. The  $Q$ -function can be interpreted as the negated energy and it has a very special semantics:  $Q(\mathbf{s}, \mathbf{a})$  stands for the total reward obtained by an agent applying action  $\mathbf{a}$  in state  $\mathbf{s}$  and then following optimal policy. Consequently, the training of the (neural network) approximation  $\hat{Q}$  of  $Q$  leverages the fact that  $Q$  is a fixed point of the so-called *Bellman operator* ([2, 27]). Furthermore, learning the  $Q$ -function is an off-policy process and the argmin-defined policy is applied only after  $Q$ -learning is completed. The setting considered in this paper is more general - the energy  $E$  lacks the semantics of the negated  $Q$ -function which enables us to bypass the separate off-policy training of  $E$ . The algorithms presented in this paper are in fact on-policy. Needless to say, our proposed ITT architectures can be in principle applied also in  $Q$ -learning which we leave for future work.

**Energy-based models:** Implicit policies can be viewed as special instantiations of energy-based models (EBMs) (see: [16, 26] for an excellent introduction to EBMs). Several impactful ML architectures have been recently reinterpreted as EBMs. Those include Transformers [31] with their attention modules resembling modern associative memory units (the latter being flagship examples of EBMs [20] implementing differentiable dictionaries via exponential energies). We mention Transformers here on purpose. ITTs can be interpreted as learning the cross-attention between the state and action-spaces with actions corresponding to keys and states to queries.

## 2 Implicit Two-Tower (ITT) policies

### 2.1 Preliminaries

As described in Section 1, we focus in this paper on the implicit policies  $\pi_\theta : \mathcal{S} \rightarrow \mathcal{A}$  from the state-space  $\mathcal{S} \subseteq \mathbb{R}^s$  to the action-space  $\mathcal{A} \subseteq \mathbb{R}^a$ , given as follows for the learnable  $\theta \in \mathbb{R}^D$ :

$$\pi_\theta(\mathbf{s}) = \operatorname{argmin}_{\mathbf{a} \in \mathcal{A}} E_\theta(\mathbf{s}, \mathbf{a}) \quad (2)$$

Here  $E_\theta : \mathcal{S} \times \mathcal{A} \rightarrow \mathbb{R}$  is the *energy-function*, usually encoded by the neural network. In the standard implicit-policy approach, the *one-tower* model (IOT), the input to this neural network is the concatenated state-action vector:  $\text{input} = [\mathbf{s}, \mathbf{a}]$ . Solving optimization problem from Eq. 2 directly is usually prohibitively expensive. Thus instead sampling strategies are often used. For the selected set  $\mathcal{A}^* = \{\mathbf{a}_1, \dots, \mathbf{a}_N\}$  of sampled actions (usually uniformly at random from  $\mathcal{A}$ ), the algorithm approximates  $\pi_\theta(\mathbf{s})$  as:  $\hat{\pi}_\theta(\mathbf{s}) = \operatorname{argmin}_{\mathbf{a} \in \mathcal{A}^*} E_\theta(\mathbf{s}, \mathbf{a})$  or applies derivative-free-optimization heuristics (see: [10]). Alternatively, the task is relaxed and instead of solving the original argmin-problem, the action  $\mathbf{a} \in \mathcal{A}^*$  is sampled from the following softmax-distribution defined on

$\mathcal{A}^*$  (the relaxation makes it feasible to backpropagate through the action-selection modules):

$$\mathbb{P}[\widehat{\pi}_\theta(\mathbf{s}) = \mathbf{a}_i] = \frac{\exp(-E_\theta(\mathbf{s}, \mathbf{a}_i))}{\sum_{\mathbf{a} \in \mathcal{A}^*} \exp(-E_\theta(\mathbf{s}, \mathbf{a}))} \quad (3)$$

All the aforementioned approaches are inherently linear in the number of sampled actions. Furthermore, sampling is usually conducted at every state-transition. Thus in practice, for computational efficiency, a small number of samples needs to be used.

## 2.2 Two towers

In the implicit two-tower (ITT) model the energy is defined as:

$$E_\theta(\mathbf{s}, \mathbf{a}) = -K(l_S^{\theta_1}(\mathbf{s}), l_A^{\theta_2}(\mathbf{a})) \quad (4)$$

for the state-tower mapping:  $l_S^{\theta_1}(\mathbf{s}) : \mathbb{R}^s \rightarrow \mathcal{L} \subseteq \mathbb{R}^d$  and action-tower mapping:  $l_A^{\theta_2}(\mathbf{a}) : \mathbb{R}^a \rightarrow \mathcal{L} \subseteq \mathbb{R}^d$ , parameterized by  $\theta_1 \in \mathbb{R}^{D_1}$  and  $\theta_2 \in \mathbb{R}^{D_2}$  respectively (usually encoded by two neural networks) as well as a fixed kernel function  $K : \mathbb{R}^d \times \mathbb{R}^d \rightarrow \mathbb{R}$ . Here  $\mathcal{L}$  stands for the common latent space for states and actions. As in the case of regular implicit policies, action selection is conducted by solving the argmin-problem or its softmax-sampling relaxation.

A particularly prominent class of kernels that can be applied are those that are increasing functions of the dot-products of their inputs, i.e.  $K(\mathbf{x}, \mathbf{y}) = f(\mathbf{x}^\top \mathbf{y})$  for some  $f : \mathbb{R} \rightarrow \mathbb{R}$ . Those include dot-product kernel, where  $f$  is an identity function as well as the softmax-kernel, where  $f(z) \stackrel{\text{def}}{=} \exp(z)$ . For those kernels the corresponding argmax-problems are trivially equivalent and reduce to the maximum-inner-product (MIP) search, but the softmax-distributions differ. For a fixed sampled set of actions  $\mathcal{A}^* = \{\mathbf{a}_1, \dots, \mathbf{a}_N\}$ , the MIP problem can be solved particularly efficiently as follows:

$$\widehat{\pi}_{\theta_1, \theta_2}(\mathbf{s}) = \mathbf{a}_{\text{argmax}(l_A^{\theta_2}(\mathcal{A}^*) l_S^{\theta_1}(\mathbf{s}))}, \quad (5)$$

where the  $i^{\text{th}}$  rows of the matrix  $l_A^{\theta_2}(\mathcal{A}^*) \in \mathbb{R}^{N \times d}$  is given as  $l_A^{\theta_2}(\mathbf{a}_i)$ . Thus brute-force computation of the action for the given state between two consecutive updates of the action-tower (or: the set of sampled actions) takes time:  $O(Nd + T_S)$ , where  $T_S$  is the time needed to compute latent representation  $l_S^{\theta_1}(\mathbf{s})$  of  $\mathbf{s}$ . Next, we examine in detail additional computational advantages of the ITTs that can further lower this cost at the price of periodic action-tower related processing.

## 2.3 Fast Maximum Inner Product & Beyond for ITTs

### 2.3.1 Signed Random Projections for fast MIP

The formulation from Equation 5 is amenable to the hashing-based relaxation. In this setting set  $\mathcal{A}^*$  is partitioned into nonempty subsets:  $\mathcal{A}_1^*, \dots, \mathcal{A}_p^*$  based on the hash-map:  $h : \mathbb{R}^d \rightarrow \mathbb{Z}^m$ , where  $\mathbb{Z}$  is the set of all integers (a given subset of the partitioning contains actions from  $\mathcal{A}^*$  with the same vector-value of the hash-map). Hashing techniques (e.g. locality-sensitive hashing) are applied on the regular basis to speed up nearest neighbor search (NNS). The MIP-formulation at first glance does not look like the NNS, but can be easily transformed to the NNS-formulation (see: [19]), leading in our case to the new definitions of the latent embeddings corresponding to actions and states:

$$\begin{aligned} \tilde{l}_A^{\theta_2}(\mathbf{a}) &= \left[ (l_A^{\theta_2}(\mathbf{a}))^\top, \sqrt{C^2 - \|l_A^{\theta_2}(\mathbf{a})\|_2^2} \right]^\top, \\ \tilde{l}_S^{\theta_1}(\mathbf{s}) &= [(l_S^{\theta_1}(\mathbf{s}))^\top, 0]^\top, \end{aligned} \quad (6)$$

where  $C$  stands for the upper bound on the length of the original latent action-representation (e.g.  $C = \max_{\mathbf{a} \in \mathcal{A}^*} \|l_A^{\theta_2}(\mathbf{a})\|_2$ ). If the nonlinearity  $g : \mathbb{R} \rightarrow \mathbb{R}$  used in the last layer of the action-tower satisfies:  $|g(x)| \leq B$  for some finite  $B > 0$ , then one can simply take:  $C = B\sqrt{d}$ .

Note that the re-formulation from Equation 6 preserves dot-products, i.e. we trivially have:

$$(\tilde{l}_A^{\theta_2}(\mathbf{a}))^\top \tilde{l}_S^{\theta_1}(\mathbf{s}) = (l_A^{\theta_2}(\mathbf{a}))^\top l_S^{\theta_1}(\mathbf{s}), \quad (7)$$

but it has a critical advantage over the previous one - the latent representations of actions have now exactly the same length  $L = C$ . Thus the original MIP problem becomes the NNS with the angular

distance. To approximate the angular distance, we will apply the Signed Random Projection (SRP) method. The method relies on the linearization of the angular kernel via random feature (RF) map mechanism ([8]). The angular kernel  $K_{\text{ang}} : \mathbb{R}^d \times \mathbb{R}^d \rightarrow \mathbb{R}$  is defined as:

$$K_{\text{ang}}(\mathbf{x}, \mathbf{y}) = 1 - \frac{2\theta_{\mathbf{x}, \mathbf{y}}}{\pi}, \quad (8)$$

where  $\theta_{\mathbf{x}, \mathbf{y}}$  is an angle between  $\mathbf{x}$  and  $\mathbf{y}$ . The key observation is that  $K_{\text{ang}}$  can be rewritten as:

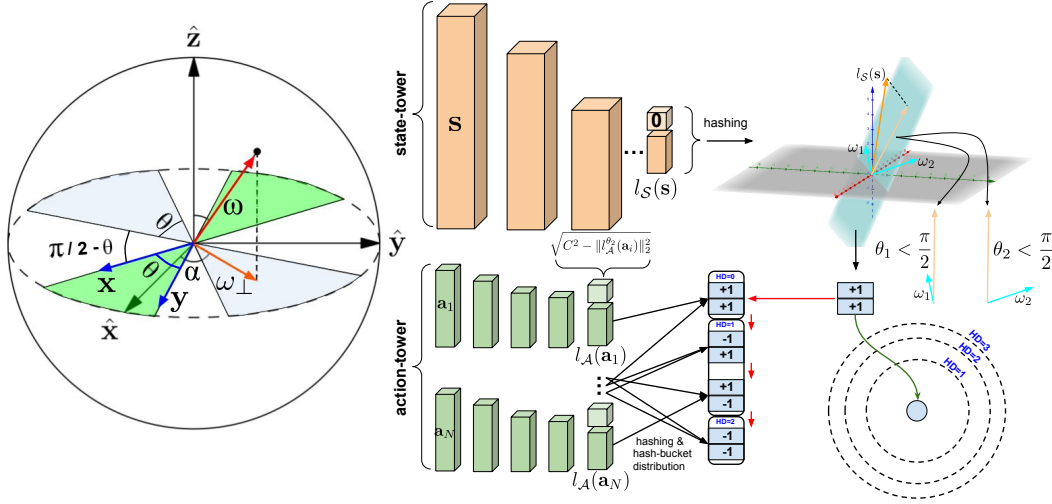


Figure 2: Pictorial description of the Signed Random Projections (SRP) LSH-hashing mechanism that can be applied in the ITT-model, in particular when larger sets of sampled actions are needed. **Left:** Explanation of the SRP-mechanism. SRP relies on the fact that the probability that  $\text{sgn}(\omega^\top \mathbf{x})\text{sgn}(\omega^\top \mathbf{y}) < 0$  is the same as the probability that the projection  $\omega_\perp$  of  $\omega \sim \mathcal{N}(0, \mathbf{I}_d)$  into the subspace spanned by  $\{\mathbf{x}, \mathbf{y}\}$  forms angle  $< \frac{\pi}{2}$  with one of  $\{\mathbf{x}, \mathbf{y}\}$  and  $> \frac{\pi}{2}$  with the other one (vector  $\omega_\perp$  inside one of the blue regions). That probability is proportional to  $\theta_{\mathbf{x}, \mathbf{y}}$  since  $\omega_\perp$  is also Gaussian. **Right:** The latent representation of the state is hashed via the projections onto a random hyperplane spanned by the Gaussian vectors  $\omega_i$ . The hash's entries are determined based on the angle  $\theta_i$  formed with vectors  $\omega_i$  (+1 for  $\theta_i < \frac{\pi}{2}$  and -1 for  $\theta_i > \frac{\pi}{2}$ ). Action hash-buckets are sorted by the Hamming distance from the state's hash and the search is conducted in that order (red arrows).

$$K_{\text{ang}}(\mathbf{x}, \mathbf{y}) = \mathbb{E} [\phi(\mathbf{x})^\top \phi(\mathbf{y})] \text{ for } \phi(\mathbf{z}) \stackrel{\text{def}}{=} \frac{1}{\sqrt{m}} (\text{sgn}(\omega_1^\top \mathbf{z}), \dots, \text{sgn}(\omega_m^\top \mathbf{z}))^\top, \quad (9)$$

where  $\omega_1, \dots, \omega_m \stackrel{\text{iid}}{\sim} \mathcal{N}(0, \mathbf{I}_d)$ . Thus each latent state/action representation can be mapped into the hashed space  $\{-1, +1\}^m \subseteq \mathbb{Z}^m$  via the mapping:  $\mathbf{z} \xrightarrow{h} (\text{sgn}(\omega_1^\top \mathbf{z}), \dots, \text{sgn}(\omega_m^\top \mathbf{z}))^\top$  and in that new space the search can occur based on the Hamming-distance from the hash-buckets corresponding to actions. The computational gains are coming from the fact that during that search, for a given input state  $\mathbf{s}$ , lots of these buckets (and thus also corresponding sets of sampled actions) will not need to be exercised at all. In our implementation, we construct  $\omega_1, \dots, \omega_m$  such that their marginal distributions are still Gaussian (thus unbiasedness of the angular kernel estimation is maintained), yet they form a block-orthogonal ensemble. This provides additional variance reduction for any number  $m$  of RFs (see: [8]). The ITT-pipeline applying SRPs is schematically presented in Fig. 2

### 2.3.2 Random Feature Trees for fast softmax-sampling

We have just shown how to further scale up MIP-optimization within ITT with the use of signed random projections. It turns out that ITT provides also a gateway to scale up softmax-sampling, as defined in Equation 3, but with the use of other hashing mechanism. We describe it below.

Let us assume that kernel  $K$  can be linearized as follows:  $K(\mathbf{x}, \mathbf{y}) = \mathbb{E}[\phi(\mathbf{x})^\top \phi(\mathbf{y})]$  for some (potentially randomized) mapping  $\phi$ . Denote by  $\psi$  the positive random feature map mechanism (FAVOR+) from [7] for linearizing the softmax-kernel (i.e.:  $\exp(\mathbf{x}^\top \mathbf{y}) = \mathbb{E}[\psi(\mathbf{x})^\top \psi(\mathbf{y})]$ ). Without loss of generality, we will assume that the size of the sampled actions set  $\mathcal{A}^*$  satisfies:  $|\mathcal{A}^*| = 2^k$  for some  $k \in \mathbb{N}$ . We construct a binary tree  $\mathcal{T}$  with nodes corresponding to the subsets of  $\mathcal{A}^*$ . In the root

we put the entire set  $\mathcal{A}^*$ . The set of actions in each non-leaf node is split into two equal-size parts (uniformly at random) and those are assigned to its two children. Leaves of the tree correspond to singleton-sets of actions.

Action assignment for a given state  $\mathbf{s}$  is conducted via the binary search in  $\mathcal{T}$  starting at its root. Whenever the algorithm reaches the leaf, its corresponding action is assigned to the input state  $\mathbf{s}$ . Assume that the algorithm reached non-leaf node  $v$  of  $\mathcal{T}$ . Denote its children as:  $v_l$  and  $v_r$  and the corresponding action-sets as  $\mathcal{A}_{v_l}^*$  and  $\mathcal{A}_{v_r}^*$  respectively. For the ITT architecture, the following is true:

$$\begin{aligned} \mathbb{P}[\widehat{\pi}_\theta(\mathbf{s}) \in \mathcal{A}_{v_l}^* | \widehat{\pi}_\theta(\mathbf{s}) \in \mathcal{A}_{v_l}^* \cup \mathcal{A}_{v_r}^*] &= \frac{\sum_{\mathbf{a} \in \mathcal{A}_{v_l}^*} \exp(-E_\theta(\mathbf{s}, \mathbf{a}))}{\sum_{\mathbf{a} \in \mathcal{A}_{v_l}^* \cup \mathcal{A}_{v_r}^*} \exp(-E(\mathbf{s}, \mathbf{a}))} = \\ &= \frac{\sum_{\mathbf{a} \in \mathcal{A}_{v_l}^*} \exp\left\{K\left(l_S^{\theta_1}(\mathbf{s}), l_A^{\theta_2}(\mathbf{a})\right)\right\}}{\sum_{\mathbf{a} \in \mathcal{A}_{v_l}^* \cup \mathcal{A}_{v_r}^*} \exp\left\{K\left(l_S^{\theta_1}(\mathbf{s}), l_A^{\theta_2}(\mathbf{a})\right)\right\}} \approx \frac{\sum_{\mathbf{a} \in \mathcal{A}_{v_l}^*} \exp\left(\phi(l_S^{\theta_1}(\mathbf{s}))^\top \phi(l_A^{\theta_2}(\mathbf{a}))\right)}{\sum_{\mathbf{a} \in \mathcal{A}_{v_l}^* \cup \mathcal{A}_{v_r}^*} \exp\left(\phi(l_S^{\theta_1}(\mathbf{s}))^\top \phi(l_A^{\theta_2}(\mathbf{a}))\right)} \approx \\ &\approx \frac{\psi(\phi(l_S^{\theta_1}(\mathbf{s})))^\top \sum_{\mathbf{a} \in \mathcal{A}_{v_l}^*} \psi(\phi(l_A^{\theta_2}(\mathbf{a})))}{\psi(\phi(l_S^{\theta_1}(\mathbf{s})))^\top \sum_{\mathbf{a} \in \mathcal{A}_{v_l}^* \cup \mathcal{A}_{v_r}^*} \psi(\phi(l_A^{\theta_2}(\mathbf{a})))} = \frac{\psi(\phi(l_S^{\theta_1}(\mathbf{s})))^\top \xi(v_l)}{\psi(\phi(l_S^{\theta_1}(\mathbf{s})))^\top (\xi(v_l) + \xi(v_r))}, \end{aligned} \quad (10)$$

where  $\xi(v) \stackrel{\text{def}}{=} \sum_{\mathbf{a} \in \mathcal{A}_v^*} \psi(\phi(l_A^{\theta_2}(\mathbf{a})))$ . We conclude that in order to decide whether to choose  $v_l$  or  $v_r$ , the algorithm just needs to sample from the binary distribution with:  $p_l = \frac{a}{a+b}, p_r = \frac{b}{a+b}$ , where  $a = \psi(\phi(l_S^{\theta_1}(\mathbf{s})))^\top \xi(v_l)$ ,  $b = \psi(\phi(l_S^{\theta_1}(\mathbf{s})))^\top \xi(v_r)$ . Thus if  $\xi(v)$  is computed for every node, this sampling can be conducted in time constant in  $N$ .

The total time of assigning the action to the input state is  $O(\log(N))$  (rather than linear) in the number of sampled actions (but linear in the number of random features). In practice, the actions do not need to be stored explicitly in the tree and in fact even the tree-structure does not need to be stored explicitly. We call the above tree the *Random Feature Tree* (or RFT) (see also: [4, 21]). The RFT can be thought of as the hierarchical hashing approach with buckets corresponding to different nodes of the tree and levels to sets of nodes within a fixed distance from the root.

**Remark 2.1.** Both: ITT-SRPs and ITT-RFTs can be applied in both: training and/or inference. For higher accuracy, one can train with the regular ITT and run inference with ITT-SRP/RFT.

**Lazy action-tower updates:** Both considered data structures: SRP- and RFT-based hashes need to be updated every time the parameters of the action-tower are updated, but provide desired speedups between consecutive updates (if the sets of chosen sampled actions do not change). Fortunately, in the ITT-model, the frequency of updates of the action-tower can be completely disentangled from the one for the state-tower. In particular, the action-tower can be updated much less frequently or with frequency decaying in time (for instance exponentially). As for many other features of the implicit policies considered here, this one is unique for the ITT model and is not present in the regular IOT.

### 3 Experiments

We conducted three experiments: (a) compared ITT with IOT and explicit policies on 15 environments from OpenAI Gym and DeepMind Control Suite (DMCS) RL libraries, (b) compared regular ITT with its SRP-version, (c) compared regular ITT with its lazy-tower version (the latter two on the subset of these environments). Additional experimental details are in the Appendix.

#### 3.1 ITTs versus IOTs and explicit policies

**ES-optimization setup.** Let  $\theta = (\theta_1^\top, \theta_2^\top)^\top \in \mathbb{R}^D$ , where  $D = D_1 + D_2$  and  $\theta_i \in \mathbb{R}^{D_i}$  for  $i = 1, 2$ . We conducted gradient-based optimization with the antithetic ES-gradient estimator applying orthogonal samples (see: [6]), defined as follows:

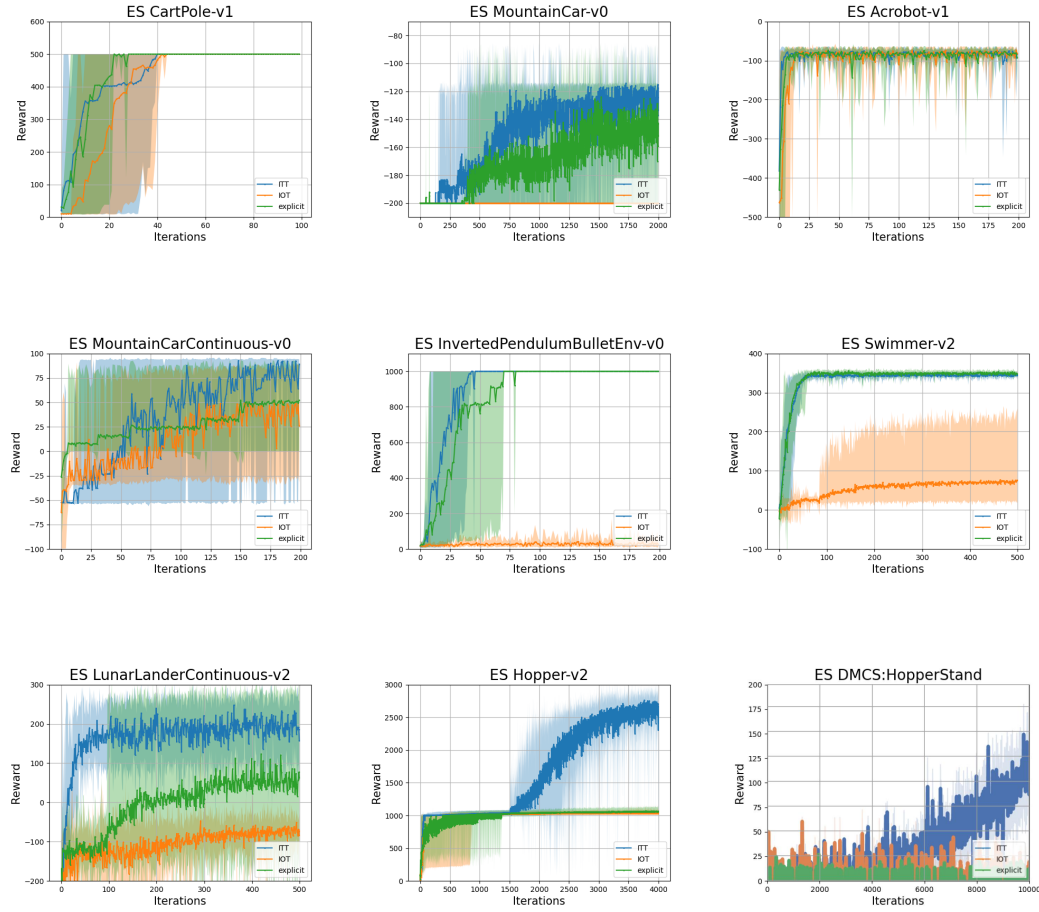
$$\widehat{\nabla}_M^{\text{AT, ort}} F_\sigma(\theta) = \frac{1}{2\sigma M} \sum_{i=1}^M (F(\theta + \sigma \varepsilon_i) \varepsilon_i - F(\theta - \sigma \varepsilon_i) \varepsilon_i), \quad (11)$$

for the hyper-parameter  $\sigma > 0$  and where  $(\varepsilon_i)_{i=1}^M$  have marginal distribution  $\mathcal{N}(\mathbf{0}, I_D)$ , and  $(\varepsilon_i)_{i=1}^M$  are conditioned to be pairwise-orthogonal. Such an ensemble of samples can always be constructed

since in all our experiments we have:  $M \leq D$ . To be more specific, for the DMCS environments we used:  $M = 500$  and for all other:  $M = D$ . At each training epoch, we were updating  $\theta$  as

$$\theta_{k+1} = \theta_k + \eta \widehat{\nabla}_M^{\text{AT, ort}} F_\sigma(\theta) \quad (12)$$

We fixed  $\eta = 0.01$  throughout the experiments. For the OpenAI Gym environments, at each transition we were sampling a set of actions  $\mathcal{A}^* = \{\mathbf{a}_1, \dots, \mathbf{a}_N\}$ , and choosing an action according to Equation 5. For the DMCS environments,  $\mathcal{A}^*$  was sampled at each iteration of the ES-optimization (independently for different ES-workers). For the environments with discrete actions, such as MountainCar-v0, we choose  $\mathcal{A}^* = \mathcal{A}$ . For the environments with continuous actions, we set  $N = 1000$  for the OpenAI Gym environments and  $N = 10000$  for the DMCS environments. Figure 3 and Table 1 illustrate the results. ITTs provide the best policies on 12 out of 15 tasks in terms of the maximum average score (see also: Appendix, Table: 6.1) and is second best on the remaining three, while having substantially faster iterations than IOTs (see: wall-clock time analysis below). For the environments from Table 1 the training curves were much less monotonic than for the other ones thus, for the clarity of the presentations, the corresponding results were given in the table.



Environment	ITT	IOT	Explicit
DMCS:Swimmer6	<b>988.26</b> $\pm$ 10.11	984.88 $\pm$ 28.05	767.44 $\pm$ 120.22
DMCS:Swimmer15	<b>995.81</b> $\pm$ 7.02	990.68 $\pm$ 0.001	935.99 $\pm$ 48.69
DMCS:FishSwim	<b>652.21</b> $\pm$ 152.07	331.73 $\pm$ 8.42	<u>470.66</u> $\pm$ 0.004

Table 1: Setting analogous to the one from Fig. 3. We present maximum average scores over  $s = 10$  random seeds together with their std. The best architecture is in bold font and the second best is underscored.

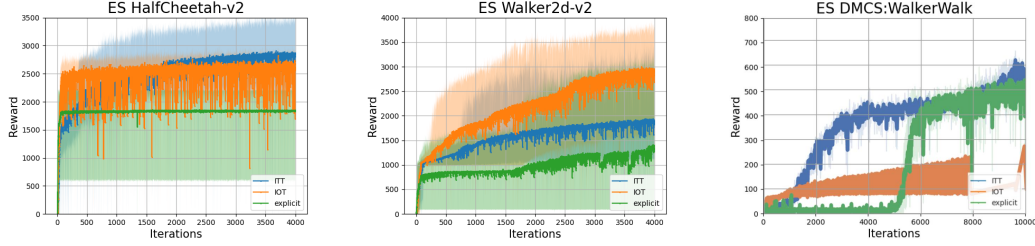


Figure 3: The comparison of the performance of different policy-architectures: ITTs, IOTs and explicit on various OpenAI Gym and DeepMind Control Suite tasks. We plot average curves obtained from  $s = 10$  seeds, and present the maximum and the minimum reward using shadowed regions. For fair comparison, we choose architectures’ sizes such that the number of trainable parameters of ITTs is comparable to but upper-bounded by that of IOTs and explicit variants (see: Appendix with additional experimental details).

**Wall-clock time.** Table 2 shows the wall-clock time (in hours on 24 CPU cores) for each policy-architecture for a selected set of environments. For each of these environments, we also include the number of training iterations. We conclude that for simpler environments (with the corresponding smaller sizes of policy-architectures) all three architectures perform similarly speed-wise. However for more complicated environments ITTs train much faster than IOTs (**26%** training time reduction for Hopper-v2, **45%** for HalfCheetah-v2 and **39%** for Walker2d-v2).

Environment	ITT	IOT	Explicit	Number of iterations
Swimmer-v2	0.17	0.18	0.11	500
LunarLanderContinuous-v2	0.06	0.06	0.08	500
Hopper-v2	2.49	3.36	2.42	4000
HalfCheetah-v2	12.94	23.61	9.95	4000
Walker2d-v2	16.88	27.49	13.41	4000

Table 2: Comparison of the wall-clock time (in hours) for different policy-architectures and a selected sample of the environments from Fig. 3.

**Neural network specifications and hyper-parameter selection.** The dimensionality of the latent state and action vector as well as the dimensionalities of the hidden layers are set to the dimensionality of the action vector for the OpenAI Gym environments and are equal to 20 for the DMCS environments. We do not use bias terms. We apply Relu activation for all the hidden layers and linear activation on the output layers, with one exception: for the Swimmer-v2 environment, we use linear activation in all layers and for all the methods. We present specifications and hyper-parameters for each method in the Appendix ( Tables 3–5 illustrate fine-tuned hyper-parameter  $\sigma$ , the dimension of the learnable  $\theta \in \mathbb{R}^D$  and the number of layers in neural networks respectively).

### 3.2 Fast ITTs with SRPs

Next we present the results for Signed Random Projections for the fast MIP-method, described in Section 2.3.1. The random projection vectors  $\omega_1, \dots, \omega_m$  have marginal distribution  $\mathcal{N}(0, \mathbf{I}_d)$  and are conditioned to be orthogonal. The orthogonality is obtained via the Gram-Schmidt orthogonalization of the iid samples (see: [8]). When  $m$  is small, to avoid having too many or too few actions in each action hash-bucket, we calculate  $b_i = \text{median}(\{\omega_i^\top \tilde{l}_{\mathcal{A}}^{\theta_1}(\mathbf{a}_j)\}_{j=1}^N)$  for each projection vector  $\omega_i$ , and map the action to the hashed space using  $\mathbf{z} \xrightarrow{h} (\text{sgn}(\omega_1^\top \mathbf{z} - b_1), \dots, \text{sgn}(\omega_m^\top \mathbf{z} - b_m))^\top$ . Figure 4 shows the comparison of the regular ITTs with ITTs applying SRPs. For HalfCheetah-v2, we use  $N = 2^{14} = 16,384$  and  $m = 6$ . For Swimmer-v2, we use  $N = 2^{10} = 1,024$  and  $m = 3$ . ITT-SRPs maintain good performance even though the hash-space is very small (of size  $2^8 = 256$  for HalfCheetah-v2 and  $2^7 = 128$  for Swimmer-v2). We chose  $C = \max_{\mathbf{a} \in \mathcal{A}^*} \|\tilde{l}_{\mathcal{A}}^{\theta_2}(\mathbf{a})\|_2$  (see: Eq. 6).

**Note:** The ITT-SRP variant from this experiment is not comparable with the IOT from Fig. 3, since in this experiment we sampled action-sets  $\mathcal{A}^*$  less frequently.



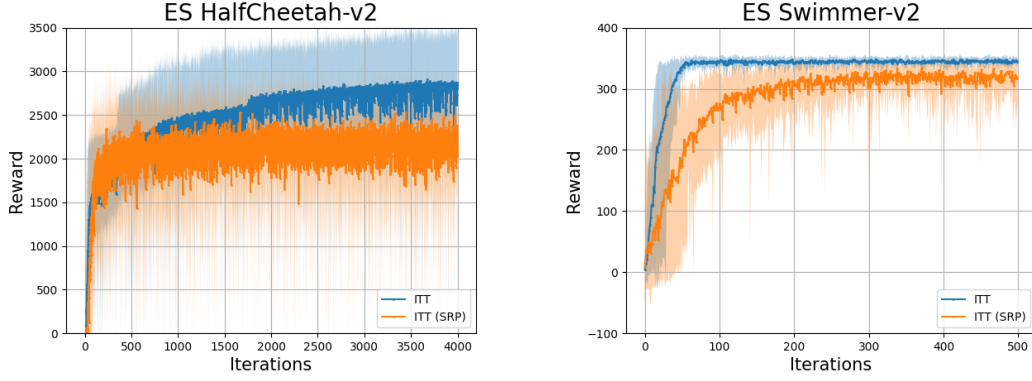


Figure 4: Comparison of vanilla ITT and ITT with Signed Random Projection for fast MIP. We plot average curves obtained from 10 seeds, and we present the maximum and the minimum reward as shadowed regions.

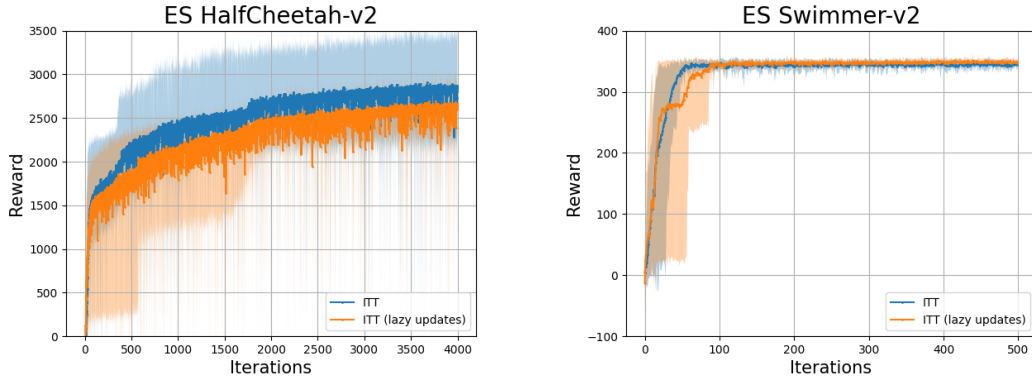


Figure 5: Comparison of the regular ITT with the ITT with lazy action-tower updates, where actions-towers are updated once every 5 iterations. We plot average curves obtained from  $s = 10$  seeds, and present the maximum and the minimum reward using shadowed regions.

### 3.3 Lazy action-tower updates

Finally, we test what happens when the action-tower is updated less frequently than the state-tower in training. In this experiment, the action tower is updated once every 5 iterations of ES-training, and the state-tower is updated at every iteration. The rest of the set up is the same as that in Section 3.1. Figure 5 shows the comparison of the regular ITT-variant with this lazy action-tower update variant. The performance is comparable, while the lazy action-tower variant has lower time complexity.

**Bootstrapping:** We observed that one can efficiently train ITTs also when the sufficiently large sampled action set  $\mathcal{A}^*$  is chosen just once (at the beginning of training) and then independently sub-sampled at each transition to provide a subset from which action will be chosen.

**Note:** We provided theoretical analysis of the antithetic estimator described at the beginning of Sec. 3, to shed light on its effectiveness and justify our choice of the ES-method. To the best of our knowledge, this is a novel insight, yet since it is not essential for the paper, we put it in the Appendix.

## 4 Limitations & broader impact of this work

Several methods presented in this work can be further extended, potentially providing additional improvements of ITTs. For instance, it seems that splitting the set of action-vectors in the given node of the RFT in such a way that the sets in its children have relatively small diameter (rather than arbitrarily) should improve the overall hierarchical hashing mechanism, yet it is not clear how to do that. Furthermore, we focus in this work on the ES-based training algorithms, yet it would be

interesting to test ITTs for a broader range of policy-optimization algorithms, potentially also for  $Q$ -learning. Even though presented methods do not have a direct negative societal impact, RL-policy training should be done responsibly, especially given its potential military applications as well as the risk associated with agents exploiting extreme exploration strategies (safety concerns).

## 5 Conclusion

We presented in this paper a new model for the architectures of the implicit policies, called the Implicit Two-Tower (ITT) model. ITTs provide substantial computational benefits over their regular Implicit One-Tower (IOT) counterparts, yet at the same time they lead to more accurate models (also as compared to the explicit policies). They are also compatible with various hashing techniques providing additional computational gains, especially if very large sets of sampled actions are needed.

## References

- [1] Peter L. Bartlett. An introduction to reinforcement learning theory: Value function methods. In Shahrar Mendelson and Alexander J. Smola, editors, *Advanced Lectures on Machine Learning, Machine Learning Summer School 2002, Canberra, Australia, February 11-22, 2002, Revised Lectures*, volume 2600 of *Lecture Notes in Computer Science*, pages 184–202. Springer, 2002.
- [2] Richard Bellman. Some applications of the theory of dynamic programming - A review. *Oper. Res.*, 2(3):275–288, 1954.
- [3] Bibit Bianchini, Mathew Halm, Nikolai Matni, and Michael Posa. Generalization bounds for implicit learning of nearly discontinuous functions. *arXiv preprint arXiv:2112.06881*, 2021.
- [4] Krzysztof Choromanski, Haoxian Chen, Han Lin, Yuanzhe Ma, Arijit Sehanobish, Deepali Jain, Michael S. Ryoo, Jake Varley, Andy Zeng, Valerii Likhoshesterov, Dmitry Kalashnikov, Vikas Sindhwani, and Adrian Weller. Hybrid random features. *ICLR 2022*, abs/2110.04367, 2021.
- [5] Krzysztof Choromanski, Aldo Pacchiano, Jack Parker-Holder, Yunhao Tang, and Vikas Sindhwani. From complexity to simplicity: Adaptive es-active subspaces for blackbox optimization. In Hanna M. Wallach, Hugo Larochelle, Alina Beygelzimer, Florence d’Alché-Buc, Emily B. Fox, and Roman Garnett, editors, *Advances in Neural Information Processing Systems 32: Annual Conference on Neural Information Processing Systems 2019, NeurIPS 2019, December 8-14, 2019, Vancouver, BC, Canada*, pages 10299–10309, 2019.
- [6] Krzysztof Choromanski, Mark Rowland, Vikas Sindhwani, Richard E. Turner, and Adrian Weller. Structured evolution with compact architectures for scalable policy optimization. In Jennifer G. Dy and Andreas Krause, editors, *Proceedings of the 35th International Conference on Machine Learning, ICML 2018, Stockholm, Sweden, July 10-15, 2018*, volume 80 of *Proceedings of Machine Learning Research*, pages 969–977. PMLR, 2018.
- [7] Krzysztof Marcin Choromanski, Valerii Likhoshesterov, David Dohan, Xingyou Song, Andreea Gane, Tamás Sarlós, Peter Hawkins, Jared Quincy Davis, Afroz Mohiuddin, Lukasz Kaiser, David Benjamin Belanger, Lucy J. Colwell, and Adrian Weller. Rethinking attention with performers. In *9th International Conference on Learning Representations, ICLR 2021, Virtual Event, Austria, May 3-7, 2021*. OpenReview.net, 2021.
- [8] Krzysztof Marcin Choromanski, Mark Rowland, and Adrian Weller. The unreasonable effectiveness of structured random orthogonal embeddings. In Isabelle Guyon, Ulrike von Luxburg, Samy Bengio, Hanna M. Wallach, Rob Fergus, S. V. N. Vishwanathan, and Roman Garnett, editors, *Advances in Neural Information Processing Systems 30: Annual Conference on Neural Information Processing Systems 2017, December 4-9, 2017, Long Beach, CA, USA*, pages 219–228, 2017.
- [9] Yilun Du, Toru Lin, and Igor Mordatch. Model-based planning with energy-based models. In Leslie Pack Kaelbling, Danica Kragic, and Komei Sugiura, editors, *3rd Annual Conference on Robot Learning, CoRL 2019, Osaka, Japan, October 30 - November 1, 2019, Proceedings*, volume 100 of *Proceedings of Machine Learning Research*, pages 374–383. PMLR, 2019.
- [10] Pete Florence, Corey Lynch, Andy Zeng, Oscar A. Ramirez, Ayzaan Wahid, Laura Downs, Adrian Wong, Johnny Lee, Igor Mordatch, and Jonathan Tompson. Implicit behavioral cloning. In Aleksandra Faust, David Hsu, and Gerhard Neumann, editors, *Conference on Robot Learning*,

- 8-11 November 2021, London, UK, volume 164 of *Proceedings of Machine Learning Research*, pages 158–168. PMLR, 2021.
- [11] Chris Gaskett, David Wettergreen, and Alexander Zelinsky. Q-learning in continuous state and action spaces. In Norman Y. Foo, editor, *Advanced Topics in Artificial Intelligence, 12th Australian Joint Conference on Artificial Intelligence, AI '99, Sydney, Australia, December 6-10, 1999, Proceedings*, volume 1747 of *Lecture Notes in Computer Science*, pages 417–428. Springer, 1999.
  - [12] David Ha and Jürgen Schmidhuber. Recurrent world models facilitate policy evolution. In Samy Bengio, Hanna M. Wallach, Hugo Larochelle, Kristen Grauman, Nicolò Cesa-Bianchi, and Roman Garnett, editors, *Advances in Neural Information Processing Systems 31: Annual Conference on Neural Information Processing Systems 2018, NeurIPS 2018, December 3-8, 2018, Montréal, Canada*, pages 2455–2467, 2018.
  - [13] Tuomas Haarnoja, Haoran Tang, Pieter Abbeel, and Sergey Levine. Reinforcement learning with deep energy-based policies. In Doina Precup and Yee Whye Teh, editors, *Proceedings of the 34th International Conference on Machine Learning, ICML 2017, Sydney, NSW, Australia, 6-11 August 2017*, volume 70 of *Proceedings of Machine Learning Research*, pages 1352–1361. PMLR, 2017.
  - [14] Deepali Jain, Ken Caluwaerts, and Atil Iscen. From pixels to legs: Hierarchical learning of quadruped locomotion. In Jens Kober, Fabio Ramos, and Claire J. Tomlin, editors, *4th Conference on Robot Learning, CoRL 2020, 16-18 November 2020, Virtual Event / Cambridge, MA, USA*, volume 155 of *Proceedings of Machine Learning Research*, pages 91–102. PMLR, 2020.
  - [15] Dmitry Kalashnikov, Alex Irpan, Peter Pastor, Julian Ibarz, Alexander Herzog, Eric Jang, Deirdre Quillen, Ethan Holly, Mrinal Kalakrishnan, Vincent Vanhoucke, and Sergey Levine. Qt-opt: Scalable deep reinforcement learning for vision-based robotic manipulation. *CoRR*, abs/1806.10293, 2018.
  - [16] Yann LeCun, Sumit Chopra, Raia Hadsell, Fu Jie Huang, and et al. A tutorial on energy-based learning. In *PREDICTING STRUCTURED DATA*. MIT Press, 2006.
  - [17] Horia Mania, Aurelia Guy, and Benjamin Recht. Simple random search of static linear policies is competitive for reinforcement learning. In Samy Bengio, Hanna M. Wallach, Hugo Larochelle, Kristen Grauman, Nicolò Cesa-Bianchi, and Roman Garnett, editors, *Advances in Neural Information Processing Systems 31: Annual Conference on Neural Information Processing Systems 2018, NeurIPS 2018, December 3-8, 2018, Montréal, Canada*, pages 1805–1814, 2018.
  - [18] Ninh Pham. Simple yet efficient algorithms for maximum inner product search via extreme order statistics. In Feida Zhu, Beng Chin Ooi, and Chunyan Miao, editors, *KDD '21: The 27th ACM SIGKDD Conference on Knowledge Discovery and Data Mining, Virtual Event, Singapore, August 14-18, 2021*, pages 1339–1347. ACM, 2021.
  - [19] Ninh D. Pham. Sublinear maximum inner product search using concomitants of extreme order statistics. *ArXiv*, abs/2012.11098, 2020.
  - [20] Hubert Ramsauer, Bernhard Schöfl, Johannes Lehner, Philipp Seidl, Michael Widrich, Lukas Gruber, Markus Holzleitner, Thomas Adler, David P. Kreil, Michael K. Kopp, Günter Klambauer, Johannes Brandstetter, and Sepp Hochreiter. Hopfield networks is all you need. In *9th International Conference on Learning Representations, ICLR 2021, Virtual Event, Austria, May 3-7, 2021*. OpenReview.net, 2021.
  - [21] Ankit Singh Rawat, Jiecao Chen, Felix X. Yu, Ananda Theertha Suresh, and Sanjiv Kumar. Sampled softmax with random fourier features. In Hanna M. Wallach, Hugo Larochelle, Alina Beygelzimer, Florence d’Alché-Buc, Emily B. Fox, and Roman Garnett, editors, *Advances in Neural Information Processing Systems 32: Annual Conference on Neural Information Processing Systems 2019, NeurIPS 2019, December 8-14, 2019, Vancouver, BC, Canada*, pages 13834–13844, 2019.
  - [22] Tim Salimans, Jonathan Ho, Xi Chen, and Ilya Sutskever. Evolution strategies as a scalable alternative to reinforcement learning. *CoRR*, abs/1703.03864, 2017.
  - [23] John Schulman, Filip Wolski, Prafulla Dhariwal, Alec Radford, and Oleg Klimov. Proximal policy optimization algorithms. *CoRR*, abs/1707.06347, 2017.

- [24] Anshumali Shrivastava and Ping Li. Asymmetric minwise hashing for indexing binary inner products and set containment. In Aldo Gangemi, Stefano Leonardi, and Alessandro Panconesi, editors, *Proceedings of the 24th International Conference on World Wide Web, WWW 2015, Florence, Italy, May 18-22, 2015*, pages 981–991. ACM, 2015.
- [25] Anshumali Shrivastava and Ping Li. Improved asymmetric locality sensitive hashing (ALSH) for maximum inner product search (MIPS). In Marina Meila and Tom Heskes, editors, *Proceedings of the Thirty-First Conference on Uncertainty in Artificial Intelligence, UAI 2015, July 12-16, 2015, Amsterdam, The Netherlands*, pages 812–821. AUAI Press, 2015.
- [26] Yang Song and Diederik P. Kingma. How to train your energy-based models. *CoRR*, abs/2101.03288, 2021.
- [27] Zhao Song, Ronald Parr, and Lawrence Carin. Revisiting the softmax bellman operator: New benefits and new perspective. In Kamalika Chaudhuri and Ruslan Salakhutdinov, editors, *Proceedings of the 36th International Conference on Machine Learning, ICML 2019, 9-15 June 2019, Long Beach, California, USA*, volume 97 of *Proceedings of Machine Learning Research*, pages 5916–5925. PMLR, 2019.
- [28] Richard S. Sutton. Reinforcement learning: Past, present and future. In Bob McKay, Xin Yao, Charles S. Newton, Jong-Hwan Kim, and Takeshi Furuhashi, editors, *Simulated Evolution and Learning, Second Asia-Pacific Conference on Simulated Evolution and Learning, SEAL’98, Canberra, Australia, November 24-27 1998, Selected Papers*, volume 1585 of *Lecture Notes in Computer Science*, pages 195–197. Springer, 1998.
- [29] Richard S. Sutton and Andrew G. Barto. *Reinforcement learning - an introduction*. Adaptive computation and machine learning. MIT Press, 1998.
- [30] Hado van Hasselt, Arthur Guez, and David Silver. Deep reinforcement learning with double q-learning. In Dale Schuurmans and Michael P. Wellman, editors, *Proceedings of the Thirtieth AAAI Conference on Artificial Intelligence, February 12-17, 2016, Phoenix, Arizona, USA*, pages 2094–2100. AAAI Press, 2016.
- [31] Ashish Vaswani, Noam Shazeer, Niki Parmar, Jakob Uszkoreit, Llion Jones, Aidan N. Gomez, Lukasz Kaiser, and Illia Polosukhin. Attention is all you need. In Isabelle Guyon, Ulrike von Luxburg, Samy Bengio, Hanna M. Wallach, Rob Fergus, S. V. N. Vishwanathan, and Roman Garnett, editors, *Advances in Neural Information Processing Systems 30: Annual Conference on Neural Information Processing Systems 2017, December 4-9, 2017, Long Beach, CA, USA*, pages 5998–6008, 2017.
- [32] Christopher J. C. H. Watkins and Peter Dayan. Technical note q-learning. *Mach. Learn.*, 8:279–292, 1992.
- [33] Wenhao Yu, Deepali Jain, Alejandro Escontrela, Atil Iscen, Peng Xu, Erwin Coumans, Sehoon Ha, Jie Tan, and Tingnan Zhang. Visual-locomotion: Learning to walk on complex terrains with vision. In Aleksandra Faust, David Hsu, and Gerhard Neumann, editors, *Conference on Robot Learning, 8-11 November 2021, London, UK*, volume 164 of *Proceedings of Machine Learning Research*, pages 1291–1302. PMLR, 2021.

## 6 Appendix

### 6.1 Additional experimental details

We present here additional experimental results containing in particular the values of the fine-tuned parameter  $\sigma$  of the ES-optimization for different policy-architectures and environments as well as the specification of the neural networks used to encode the policies and the total number of trainable parameters. We also present maximum average scores together with their corresponding standard deviations (over  $s = 10$  different seeds) for all 15 environments tested in the paper. We include the code and instructions how to use it at <https://anonymous.4open.science/r/itt-7262/README.md>

Environment	ITT	IOT	Explicit
Swimmer-v2	1	1	1
LunarLanderContinuous-v2	1	1	1
Hopper-v2	1	1	1
HalfCheetah-v2	1	1	0.5
Walker2d-v2	0.5	0.5	0.5
CartPole-v1	1	1	1
MountainCar-v0	1	1	1
Acrobot-v1	1	1	1
MountainCarContinuous-v0	1	1	1
InvertedPendulumBulletEnv-v0	1	1	1
DMCS:FishSwim	0.1	0.1	0.1
DMCS:Swimmer6	0.1	0.1	0.1
DMCS:Swimmer15	0.1	0.1	0.1
DMCS:HopperStand	0.1	0.1	0.1
DMCS:WalkerWalk	0.1	0.1	0.1

Table 3: Fine-tuned hyper-parameter  $\sigma$ , used in ES gradient estimator calculations (Equation 11) for different environments and different policy-architectures.

Environment	ITT	IOT	Explicit
Swimmer-v2	20	22	20
LunarLanderContinuous-v2	20	22	20
Hopper-v2	42	45	42
HalfCheetah-v2	282	288	282
Walker2d-v2	246	252	246
CartPole-v1	6	7	6
MountainCar-v0	4	5	4
Acrobot-v1	8	9	8
MountainCarContinuous-v0	3	4	3
InvertedPendulumBulletEnv-v0	12	13	12
DMCS:FishSwim	2180	2200	2180
DMCS:Swimmer6	2200	2220	2200
DMCS:Swimmer15	3100	3120	3100
DMCS:HopperStand	1980	2000	1980
DMCS:WalkerWalk	2200	2220	2200

Table 4: The dimensionality of the learnable  $\theta \in \mathbb{R}^D$  for different environments and different policy-architectures.

### 6.2 Theoretical Results

We start with introducing notations that help us simplify the proofs.

Environment	ITT state tower	ITT action tower	IOT	Explicit
Swimmer-v2	1	1	2	2
LunarLanderContinuous-v2	1	1	2	2
Hopper-v2	1	1	2	2
HalfCheetah-v2	4	2	6	6
Walker2d-v2	3	2	5	5
CartPole-v1	2	1	3	3
MountainCar-v0	2	1	3	3
Acrobot-v1	2	1	3	3
MountainCarContinuous-v0	1	1	2	2
InvertedPendulumBulletEnv-v0	1	1	2	2
DMCS:FishSwim	3	1	5	5
DMCS:Swimmer6	3	1	5	5
DMCS:Swimmer15	3	1	5	5
DMCS:HopperStand	3	1	5	5
DMCS:WalkerWalk	3	1	5	5

Table 5: The number of layers of the neural networks encoding different architectures for different environments.

Environment	ITT	IOT	Explicit
Swimmer-v2	$344.13 \pm 5.18$	$75.54 \pm 88.05$	<b><math>347.67 \pm 5.74</math></b>
LunarLanderContinuous-v2	<b><math>157.38 \pm 71.81</math></b>	$-72.72 \pm 26.98$	$62.85 \pm 176.36$
Hopper-v2	<b><math>2670.37 \pm 225.53</math></b>	$1036.52 \pm 29.16$	$1060.89 \pm 40.71$
HalfCheetah-v2	<b><math>2866.02 \pm 416.81</math></b>	$2696.29 \pm 274.51$	$1845.64 \pm 441.96$
Walker2d-v2	<u><math>1897.87 \pm 498.86</math></u>	<b><math>2909.85 \pm 621.45</math></b>	$1346.93 \pm 906.33$
CartPole-v1	<b><math>500.00 \pm 0.00</math></b>	<b><math>500.00 \pm 0.00</math></b>	<b><math>500.00 \pm 0.00</math></b>
MountainCar-v0	<b><math>-133.50 \pm 27.10</math></b>	$-200.00 \pm 0.00$	$-143.40 \pm 37.12$
Acrobot-v1	$-82.60 \pm 11.93$	<b><math>-82.00 \pm 8.54</math></b>	$-92.10 \pm 21.41$
MountainCarContinuous-v0	<b><math>89.17 \pm 8.97</math></b>	$25.96 \pm 53.61$	$52.34 \pm 42.74$
InvertedPendulumBulletEnv-v0	<b><math>1000.00 \pm 0.00</math></b>	$27.10 \pm 12.70$	<b><math>1000.00 \pm 0.00</math></b>
DMCS:Swimmer6	<b><math>988.26 \pm 10.11</math></b>	<u><math>984.88 \pm 28.05</math></u>	$767.44 \pm 120.22$
DMCS:Swimmer15	<b><math>995.81 \pm 7.02</math></b>	<u><math>990.68 \pm 0.001</math></u>	$935.99 \pm 48.69$
DMCS:FishSwim	<b><math>652.21 \pm 152.07</math></b>	$331.73 \pm 8.42$	<u><math>470.66 \pm 0.004</math></u>

Table 6: Setting analogous to the one from Fig. 3. We present maximum average scores over  $s = 10$  random seeds together with their std. The best architecture is in bold font and the second best is underscored.

**Definition 1** (AT and FD ES-gradient estimator). *The antithetic ES-gradient estimator and the forward finite difference ES-gradient estimator applying orthogonal samples are defined as*

$$\hat{\nabla}_M^{\text{AT}, \text{ort}} F_\sigma(\theta) := \frac{1}{2\sigma M} \sum_{i=1}^M F^{\text{AT}(i)} \quad \text{where} \quad F^{\text{AT}(i)} := F(\theta + \sigma \varepsilon_i) \varepsilon_i - F(\theta - \sigma \varepsilon_i) \varepsilon_i \quad (13)$$

$$\hat{\nabla}_M^{\text{FD}, \text{ort}} F_\sigma(\theta) := \frac{1}{\sigma M} \sum_{i=1}^M F^{\text{FD}(i)} \quad \text{where} \quad F^{\text{FD}(i)} := F(\theta + \sigma \varepsilon_i) \varepsilon_i - F(\theta) \varepsilon_i, \quad (14)$$

where  $(\varepsilon_i)_{i=1}^M$  have marginal distribution  $\mathcal{N}(\mathbf{0}, I_D)$ , and  $(\varepsilon_i)_{i=1}^M$  are conditioned to be pairwise-orthogonal.

**Definition 2** (Gaussian smoothing). *The Gaussian smoothing of  $F(x)$  is defined as*

$$F_\sigma(\theta) = \frac{1}{\kappa} \int F(\theta + \sigma \varepsilon) e^{-\frac{1}{2} \|\varepsilon\|_2^2} d\varepsilon, \quad \text{where } \kappa = (2\pi)^{d/2}, \quad (15)$$

and its gradient is

$$\nabla F_\sigma(\theta) = \frac{1}{\sigma \kappa} \int F(\theta + \sigma \varepsilon) e^{-\frac{1}{2} \|\varepsilon\|_2^2} \varepsilon d\varepsilon. \quad (16)$$

**Assumption 1.** Assume  $F(\cdot)$  is quadratic. Under this assumption, the gradient  $\nabla F(\theta)$  and the Hessian  $\nabla^2 F(\theta)$  exist for any  $\theta \in \mathbb{R}^D$ , and

$$F(\theta + \sigma \varepsilon) = F(\theta) + \sigma \nabla F(\theta)^\top \varepsilon + \frac{\sigma^2}{2} \varepsilon^\top \nabla^2 F(\theta) \varepsilon.$$

**Theorem 1.** Suppose Assumption 1 holds. The mean squared error of the AT ES-gradient estimator applying orthogonal samples is

$$\begin{aligned}\text{MSE}\left(\hat{\nabla}_M^{\text{AT,ort}} F_\sigma(\theta)\right) &:= \mathbb{E}\left[\left\|\hat{\nabla}_M^{\text{AT,ort}} F_\sigma(\theta) - \nabla F_\sigma(\theta)\right\|_2^2\right] \\ &= \frac{1}{M} \mathbb{E}\left[\left\|(\nabla F(\theta)^\top \varepsilon)\varepsilon\right\|_2^2\right] - \|\nabla F_\sigma(\theta)\|_2^2.\end{aligned}$$

The mean squared error of the FD ES-gradient estimator applying orthogonal samples is

$$\begin{aligned}\text{MSE}\left(\hat{\nabla}_M^{\text{FD,ort}} F_\sigma(\theta)\right) &:= \mathbb{E}\left[\left\|\hat{\nabla}_M^{\text{FD,ort}} F_\sigma(\theta) - \nabla F_\sigma(\theta)\right\|_2^2\right] \\ &= \frac{1}{M} \mathbb{E}\left[\left\|(\nabla F(\theta)^\top \varepsilon + \frac{\sigma^2}{2} \varepsilon^\top \nabla^2 F(\theta) \varepsilon)\varepsilon\right\|_2^2\right] - \|\nabla F_\sigma(\theta)\|_2^2.\end{aligned}$$

Since we have orthogonal samples, we have the following Lemma.

**Lemma 1.** Assume  $M \leq D$ , we have

$$\begin{aligned}\text{MSE}\left(\hat{\nabla}_M^{\text{AT,ort}} F_\sigma(\theta)\right) &= \frac{D+2}{M} \|\nabla F(\theta)\|_2^2 - \|\nabla F_\sigma(\theta)\|_2^2 \\ \text{MSE}\left(\hat{\nabla}_M^{\text{FD,ort}} F_\sigma(\theta)\right) &= \frac{D+2}{M} \|\nabla F(\theta)\|_2^2 + \frac{(D+4)\sigma^4}{4M} \|\nabla^2 F(\theta)\|_F^2 \\ &\quad + \frac{(D+2)\sigma^4}{M} \left(\sum_{i=1}^D \nabla^2 F(\theta)_{ii}^2\right) - \|\nabla F_\sigma(\theta)\|_2^2,\end{aligned}$$

and therefor

$$\begin{aligned}&\text{MSE}\left(\hat{\nabla}_M^{\text{FD,ort}} F_\sigma(\theta)\right) - \text{MSE}\left(\hat{\nabla}_M^{\text{AT,ort}} F_\sigma(\theta)\right) \\ &= \frac{(D+4)\sigma^4}{4M} \|\nabla^2 F(\theta)\|_F^2 + \frac{(D+2)\sigma^4}{M} \left(\sum_{i=1}^D \nabla^2 F(\theta)_{ii}^2\right).\end{aligned}$$

The proofs of Theorem 1 and Lemma 1 are at the end of Section 6.2.

**Remark 6.1.** Suppose Assumption 1 holds. We observe that evaluating  $\hat{\nabla}_M^{\text{AT,ort}} F_\sigma(\theta)$  requires  $2M$  queries of  $F(\cdot)$  and evaluating  $\hat{\nabla}_M^{\text{FD,ort}} F_\sigma(\theta)$  requires only  $M+1$  queries of  $F(\cdot)$ . Consequently, FD-gradient estimator is preferred when  $\sigma^4 \|\nabla^2 F(\theta)\|_F^2 \ll \|\nabla F(\theta)\|_2^2$ , and AT-gradient estimator is preferred when  $\sigma^4 \|\nabla^2 F(\theta)\|_F^2 \gg \|\nabla F(\theta)\|_2^2$ , which is highly likely when  $\sigma$  is large.

**Remark 6.2.** Theorem 1 and Lemma 1 can be extended to general functions  $F(\cdot)$ , by taking higher order Taylor polynomials of  $F(\cdot)$ .

*proof of Theorem 1. AT ES-gradient estimator.*

$$\begin{aligned}\text{MSE}\left(\hat{\nabla}_M^{\text{AT,ort}} F_\sigma(\theta)\right) &= \mathbb{E}\left[\left\|\frac{1}{M} \sum_{i=1}^M F^{AT(i)} - \nabla F_\sigma(\theta)\right\|_2^2\right] \\ &= \mathbb{E}\left[\left\|\frac{1}{M} \sum_{i=1}^M F^{AT(i)}\right\|_2^2\right] - \|\nabla F_\sigma(\theta)\|_2^2\end{aligned}$$

The first term is

$$\begin{aligned}\mathbb{E}\left[\left\|\frac{1}{M} \sum_{i=1}^M F^{AT(i)}\right\|_2^2\right] &= \frac{1}{M^2} \left(\sum_{i=1}^M \mathbb{E}\left[\left\|F^{AT(i)}\right\|_2^2\right] + \sum_{i \neq j} \mathbb{E}\left[\langle F^{AT(i)}, F^{AT(j)} \rangle\right]\right) \\ &= \frac{1}{M^2} \left(\sum_{i=1}^M \mathbb{E}\left[\left\|F^{AT(i)}\right\|_2^2\right]\right) = \frac{1}{M^2} \left(\sum_{i=1}^M \mathbb{E}\left[\left\|\frac{1}{2\sigma}(F(\theta + \sigma\varepsilon_i)\varepsilon_i - F(\theta - \sigma\varepsilon_i)\varepsilon_i)\right\|_2^2\right]\right) \\ &= \frac{1}{M} \mathbb{E}\left[\left\|\frac{1}{2\sigma}(F(\theta + \sigma\varepsilon)\varepsilon - F(\theta - \sigma\varepsilon)\varepsilon)\right\|_2^2\right] = \frac{1}{M} \mathbb{E}\left[\left\|(\nabla F(\theta)^\top \varepsilon)\varepsilon\right\|_2^2\right],\end{aligned}$$

where the second equality is by orthogonality of  $\varepsilon_i$ ; the fourth equality is because  $\varepsilon_i$  are i.i.d.; the last equality is by Assumption 1.

**FD ES-gradient estimator.** For simplicity of presentation, we abbreviate the first few steps, which are the same as that of the AT ES-gradient estimator.

$$\begin{aligned} & \frac{1}{M^2} \left( \sum_{i=1}^M \mathbb{E} \left[ \left\| F^{FD(i)} \right\|_2^2 \right] \right) = \frac{1}{M^2} \left( \sum_{i=1}^M \mathbb{E} \left[ \left\| \frac{1}{\sigma} (F(\theta + \sigma \varepsilon_i) \varepsilon_i - F(\theta) \varepsilon_i) \right\|_2^2 \right] \right) \\ &= \frac{1}{M} \mathbb{E} \left[ \left\| \frac{1}{\sigma} (F(\theta + \sigma \varepsilon) \varepsilon - F(\theta) \varepsilon) \right\|_2^2 \right] = \frac{1}{M} \mathbb{E} \left[ \left\| \varepsilon (\nabla F(\theta)^\top \varepsilon + \frac{\sigma^2}{2} \varepsilon^\top \nabla^2 F(\theta) \varepsilon) \right\|_2^2 \right], \end{aligned}$$

where the second equality is because  $\varepsilon_i$  are i.i.d., and the third equality is by Assumption 1.  $\square$

*Proof of Lemma 1. AT ES-gradient estimator.*

$$\begin{aligned} & \mathbb{E} \left[ \left\| (\nabla F(\theta)^\top \varepsilon) \varepsilon \right\|_2^2 \right] = \sum_{i,j,k} \nabla F(\theta)_i \nabla F(\theta)_j \mathbb{E} [\varepsilon_i \varepsilon_j \varepsilon_k^2] = \sum_{i,k} \nabla F(\theta)_i^2 \mathbb{E} [\varepsilon_i^2 \varepsilon_k^2] \\ &= \sum_{i=1}^D \nabla F(\theta)_i^2 \mathbb{E} [\varepsilon_i^4] + \sum_{i=1}^D \nabla F(\theta)_i^2 \sum_{k \neq i} \mathbb{E} [\varepsilon_i^2 \varepsilon_k^2] = (D+2) \|\nabla F(\theta)\|_2^2, \end{aligned}$$

where the second equality is because odd moments of Gaussian r.v.s are zero. By Theorem 1, we have

$$\begin{aligned} \text{MSE} \left( \hat{\nabla}_M^{\text{AT,ort}} F_\sigma(\theta) \right) &:= \mathbb{E} \left[ \left\| \hat{\nabla}_N^{\text{AT,ort}} F_\sigma(\theta) - \nabla F_\sigma(\theta) \right\|_2^2 \right] \\ &= \frac{1}{M} \mathbb{E} \left[ \left\| (\nabla F(\theta)^\top \varepsilon) \varepsilon \right\|_2^2 \right] - \|\nabla F_\sigma(\theta)\|_2^2 = \frac{D+2}{M} \|\nabla F(\theta)\|_2^2 - \|\nabla F_\sigma(\theta)\|_2^2. \end{aligned}$$

**FD ES-gradient estimator.**

$$\begin{aligned} & \mathbb{E} \left[ \left\| \varepsilon (\nabla F(\theta)^\top \varepsilon + \frac{\sigma^2}{2} \varepsilon^\top \nabla^2 F(\theta) \varepsilon) \right\|_2^2 \right] \\ &= \mathbb{E} \left[ \left\| \left( \sum_{i=1}^D \nabla F(\theta)_i \varepsilon_i + \frac{\sigma^2}{2} \sum_{i=1}^D \sum_{j=1}^D \varepsilon_i \nabla^2 F(\theta)_{ij} \varepsilon_j \right) \varepsilon \right\|_2^2 \right] \\ &= \mathbb{E} \left[ \sum_{k=1}^D \varepsilon_k^2 \left( \sum_{i=1}^D \nabla F(\theta)_i \varepsilon_i + \frac{\sigma^2}{2} \sum_{i=1}^D \sum_{j=1}^D \nabla^2 F(\theta)_{ij} \varepsilon_j \right)^2 \right] \\ &= \sum_{i,j,k} \nabla F(\theta)_i \nabla F(\theta)_j \mathbb{E} [\varepsilon_i \varepsilon_j \varepsilon_k^2] + \sum_{i,j,k,l} \mathbb{E} [\varepsilon_k^2 \nabla F(\theta)_i \varepsilon_i \sigma^2 \varepsilon_j \varepsilon_l \nabla^2 F(\theta)_{jl}] \\ &\quad + \sum_{i,j,k} \mathbb{E} \left[ \varepsilon_k^2 \frac{\sigma^4}{4} \varepsilon_i^2 \varepsilon_j^2 \nabla^2 F(\theta)_{ij}^2 \right], \end{aligned}$$

The second term above equals zero, because the odd moments of Gaussian random variables are zero (in a degree 5 polynomial of Gaussian r.v.s, one term must be raised to an odd power); the first term equals  $(D+2) \|\nabla F(\theta)\|_2^2$  by the same argument as for the AT ES-gradient estimator; the third term



is

$$\begin{aligned}
\sum_{i,j,k} \mathbb{E} \left[ \varepsilon_k^2 \frac{\sigma^4}{4} \varepsilon_i^2 \varepsilon_j^2 \nabla^2 F(\theta)_{ij}^2 \right] &= \frac{\sigma^4}{4} \left( 15 \sum_i \nabla^2 F(\theta)_{ii}^2 \right) + \frac{\sigma^4}{4} 3(D-1) \sum_i \nabla^2 F(\theta)_{ii}^2 \\
&+ \frac{\sigma^4}{4} 3 \sum_i \sum_{j \neq i} \nabla^2 F(\theta)_{ij}^2 + \frac{\sigma^4}{4} 3 \sum_j \sum_{i \neq j} \nabla^2 F(\theta)_{ij}^2 + \frac{\sigma^4}{4} (D-2) \left( \sum_i \sum_{j \neq i} \nabla^2 F(\theta)_{ij}^2 \right) \\
&= \frac{(D+4)\sigma^4}{4} \|\nabla^2 F(\theta)\|_F^2 + \frac{(8+4D)\sigma^4}{4} \sum_{i=1}^D \nabla^2 F(\theta)_{ii}^2,
\end{aligned}$$

where in the first equality, the five terms correspond to  $i = j = k$ ,  $i = j \neq k$ ,  $i = k \neq j$ ,  $j = k \neq i$  and distinct  $i, j, k$  respectively.

□